Pis'ma v ZhETF, vol. 73, iss. 12, pp. 746 – 750 © 2001 June 25

Remanent states of small ferromagnetic cylinder

V. Ternovsky[1)], *B. Luk'yanchuk, J. P. Wang*

Data Storage Institute of Singapore, 117608 Singapore

Submitted 7 May 2001

Resubmitted 21 May 2001

The internal magnetic structures of a cylinder are computed without prior assumption of the axial symmetry. Three-dimensional magnetostatic solution is presented. Detailed distribution of the magnetization is obtained through numerical integration of the Landau-Lifshitz equation with the demagnetization field. Various entry conditions were used. Materials with small uniaxial anisotropy demonstrate typically vortex structures, while the higher anisotropy leads to formation of concentric cylindrical magnetic bubbles inside the cylinder and monodomain flower state.

PACS: 75.60.Ch

The problem of the shaped body magnetization under the action of some initial magnetic field refers to the well-known problem in magnetism [1, 2], however, until now it is insufficiently analyzed. Solution of this problem is important for the design of high-density magnetic recording media or magnetic random access memory. The modern line in these device fabrications is usage of patterned magnetic recording media with nanoscale sizes, where each element stores one bit of data (see, e.g. [3]). This patterning permits to enlarge the signal to noise ratio. The elements in arrays are designed so that an element's magnetostatic interactions with its neighbors will be small in comparison to its coercivity [4]. Such patterned media have been proposed for high-density data storage (above 500 Gbt/in^2), see [4] and Refs therein.

Particles with dimension of about 100 nm (and below) are usually too small to show well-developed domain structure, but show a variety of nonuniform magnetization configurations. These remanent states depend on the properties of magnetic body and its geometry, as well as the magnetization prehistory.

The first problem of this kind, which has been explored in details, refers to the magnetic states of small cubic particles [1, 2, 5, 6]. The analysis shows that magnetic states in small ferromagnetic cube can be classified in terms of some elementary structures, namely flower state (single domain), two domains, vortex and twisted vortex states. The phase diagram of these states with zero magnetic fields was recently calculated in coordinates relative to exchange interaction and the uniaxial anisotropy [6]. These remanent states were identified experimentally, using magnetic force microscopy [7], Kerr microscopy [8] and other high-resolution magnetic imaging methods [9]. The reason for variety of magnetization configuration in cubic particle is related to its high symmetry.

Although the high-density (of 100 Gbt/in^2) writing and reading on perpendicular recording media patterned by square islands was recently demonstrated [10], many researchers do not consider the cubic (or thin square) particles as optimal for magnetic recording. Thus, the particles with lower symmetry are intensively discussed. Among the shapes, which were experimentally analyzed, are elliptical [11], conical [12], cylindrical [13] and spherical [14] particles. Analysis of 3D magnetic structures for these particle shapes is more complex than for cubic particles (see, e.g. comments in [1]).

Below we suggest an effective iterative solver for cylindrical particles. A realistic representation of ferromagnetic cylinder assumes its finite height, $z = h$, and radius, $r = a$, i.e. 3D case is considered. The parameters chosen in numerical calculations correspond to those commonly used for patterned magnetic media [15]. The easy axis is the axis of the cylinder (z).

The magnetic structure is calculated by solving of the Landau-Lifshitz-Gilbert (LLG) equation (see, e.g. in [1, 2, 16]) for natural movement of magnetization. For the convenience in the calculations, we consider $\mathbf{M}$ as normalized (by M_s, which is saturated value) magnetization vector. Thus, the normalized LLG equation is presented by [1]

$$(1+\alpha^2)\frac{d\mathbf{M}}{dt} = \mathbf{H}\times\mathbf{M} - \alpha\mathbf{M}\times(\mathbf{M}\times\mathbf{H}), \quad \mathbf{M}|_{t=0} = \mathbf{M}_0, \tag{1}$$

where α is dimensionless damping factor, introduced to specify quasi-local dissipative phenomena. This factor depends nonlinearly on the magnetization [17], but for

[1)] e-mail: vladimir@dsi.nus.edu.sg

the search of the magnetization structures, this dependence can be omitted. The "classical" form of LLG equation (1) does not include gradient dissipation terms [18]. These terms play an important role for the line broadening in ferromagnetic resonance, however they are unimportant for the analysis of magnetization structures.

Value $\mathbf{H}$ in (1) presents the local effective magnetic field. This field is given by the sum of anisotropy, exchange and demagnetization fields:

$$\mathbf{H} = -4\pi Q \mathbf{M}_{\perp} + \mathbf{H}^{(ex)} + \mathbf{H}^{(m)}. \qquad (2)$$

Here $Q = K_a/2\pi M_s^2$, K_a is the anisotropy constant. Laplacian within the expression for exchange field, $\mathbf{H}^{(ex)} = 2\Delta\mathbf{M}$, is also written in dimensionless form, the characteristic exchange length, $\lambda = \sqrt{A}/M_s$ (A is the exchange stiffness constant), is used to normalize the derivations.

The main complexity refers to the demagnetizing field, $\mathbf{H}^{(m)}$, created by $\mathbf{M}$. This field can be defined from the magnetostatic problem [16]:

$$\operatorname{rot}\mathbf{H}^{(m)} = 0, \quad \operatorname{div}(\mathbf{H}^{(m)} + 4\pi\mathbf{M}) = 0, \qquad (3)$$

with proper jump (absence of magnetization out the particle) and boundary conditions (continuity of the tangential component of $\mathbf{H}$ and normal component of the magnetic induction $\mathbf{B}$). It is convenient to rewrite Maxwell equations (3) using potential U, $\mathbf{H}^{(m)} = -\operatorname{grad} U$. This potential can be presented in the form $U = F + V$, where F and V functions fulfill, the Poisson and Laplace equations:

$$\Delta F = 4\pi \operatorname{div}\mathbf{M}, \quad \Delta V = 0. \qquad (4)$$

The Poisson equation (4) is solved with zero boundary condition on the surface. Boundary condition for the Laplace equation provides continuity of the magnetic induction:

$$F|_S = 0, \quad V|_S = \oint\!\!\!\oint_S \left[-\frac{1}{4\pi}\frac{\partial F(\mathbf{r}_1)}{\partial \mathbf{n}} + \mathbf{M}(r_1)\mathbf{n}\right]\frac{d\mathbf{r}_1}{|\mathbf{r}-\mathbf{r}_1|}. \qquad (5)$$

Unit vector $\mathbf{n}$ in (5) characterized the normal to the surface. Micromagnetic equations are typically solved by finite difference technique, using some equidistant 3D grid in Cartesian coordinates [19]. This technique is more suitable for parallelepiped particle shapes, although the problem of the corner singularities [20, 21] is open with this technique.

We suggest the iterative technique, which permits to solve equations (1)–(5) for cylinder. We used the analytical solution of Maxwell equation (4), (5) for fixed distribution of magnetization $\mathbf{M}$. The solution is written in cylindrical coordinates, $\{r, \varphi, z\}$, where z is the cylinder axis. Having in mind periodical conditions, $U(r, \varphi + 2\pi, z) = U(r, \varphi, z)$ one can use the Fourier series:

$$U(r,\varphi,z) = \frac{1}{2}[V_0(r,z) + W_0(r,z)] + \sum_{k=1}^{\infty}[(V_k + W_k)\cos k\varphi + (S_k + E_k)\sin k\varphi], \qquad (6)$$

$$\mathbf{M}(r,\varphi,z) = \frac{1}{2}\mathbf{A}_0(r,z) + \sum_{k=1}^{\infty}[\mathbf{A}_k(r,z)\cos k\varphi + \mathbf{B}_k(r,z)\sin k\varphi]. \qquad (7)$$

Here we do not assume the axial symmetry of solution in advance. The relation of the coefficients in (6) to Fourier components of magnetization vector (7) can be found with the Hankel and Fourier transforms (with respect to r and z coordinates):

$$\begin{aligned}
V_k(r,z) &= \int_0^{\infty} ds\, sJ_k(sr)\widetilde{V}_k(s,z),\\
S_k(r,z) &= \int_0^{\infty} ds\, sJ_k(sr)\widetilde{S}_k(s,z),\\
\widetilde{V}_k(s,z) &= \frac{1}{2}\int_0^{z} dz_1 e^{-s(z-z_1)}\Pi_k(s,z_1) - \\
&\quad -\frac{1}{2}\int_z^{h} dz_1 e^{s(z-z_1)}\Pi_k(s,z_1),\\
\widetilde{S}_k(s,z) &= \frac{1}{2}\int_0^{z} dz_1 e^{-s(z-z_1)}T_k(s,z_1) - \\
&\quad -\frac{1}{2}\int_z^{h} dz_1 e^{s(z-z_1)}T_k(s,z_1),\\
\Pi_k(s,z) &= 4\pi\int_0^{\infty} dr_1 r_1 J_k(sr_1)A_{kz}(r_1,z),\\
T_k(s,z) &= 4\pi\int_0^{\infty} dr_1 r_1 J_k(sr_1)B_{kz}(r_1,z),
\end{aligned} \qquad (8)$$

where A_{kz} and B_{kz} are the z-components of the corresponding vector coefficients in (7). By a similar way, the coefficients W_k and E_k are expressed by

$$W_k(r,z) = \frac{1}{\pi}\int_0^{\infty}\int_0^{\infty} d\omega d\xi \cos\omega(\xi - z)\widetilde{W}_k(\omega, r, \xi),$$

$$E_k(r,z) = \frac{1}{\pi}\int_0^{\infty}\int_0^{\infty} d\omega d\xi \cos\omega(\xi - z)\widetilde{E}_k(\omega, r, \xi),$$

$$\widetilde{W}_k(\omega,r,\xi) = -4\pi K_k(\omega r)\int\limits_0^r dr_1\{k[B_{k\varphi}(r_1,\xi)-$$

$$-A_{kr}(r_1,\xi)]I_k(\omega r_1) - r\omega A_{kr}(r_1,\xi)I_{k+1}(\omega r_1)\}-$$

$$-4\pi I_k(\omega r)\int\limits_r^a dr_1\{k[B_{k\varphi}(r_1,\xi)-$$

$$-A_{kr}(r_1,\xi)]K_k(\omega r_1) + r\omega A_{kr}(r_1,\xi)K_{k+1}(\omega r_1)\}, \quad (9)$$

$$\widetilde{E}_k = 4\pi K_k(\omega r)\int\limits_0^r dr_1\{k[A_{k\varphi}(r_1,\xi)+$$

$$+B_{kr}(r_1,\xi)]I_k(\omega r_1) + r\omega B_{kr}(r_1,\xi)I_{k+1}(\omega r_1)\}+$$

$$+4\pi I_k(\omega r)\int\limits_r^a dr_1\{k[A_{k\varphi}(r_1,\xi)+$$

$$+B_{kr}(r_1,\xi)]K_k + (\omega r_1) - r\omega B_{kr}(r_1,\xi)K_{k+1}(\omega r_1)\},$$

where J_k, K_k, I_k are the Bessel functions.

To combine this result with LLG equation, we use the solution of equation (1) with fixed effective field and perform iteratively one time step $(n, n+1)$ in the fixed grid point $\{r_i, \varphi_j, z_k\}$:

$$\mathbf{M}(t) = \frac{1}{C(t_n,t)}[\mathbf{H}_1(t_n,t) + \mathbf{H}_2(t_n,t)],$$

$$\mathbf{H}_1 = \left\{|\mathbf{H}| + \mathbf{H}\mathbf{M}_n+\right.$$

$$\left.+(\mathbf{H}\mathbf{M}_n - |\mathbf{H}|)\exp\left[-\frac{2\alpha}{1+\alpha^2}F(t_n,t)\right]\right\}\mathbf{H},$$

$$\mathbf{H}_2 = 2\exp\left[-\frac{\alpha}{1+\alpha^2}F(t_n,t)\right]\times \quad (10)$$

$$\times\left\{|\mathbf{H}|\sin\left[\frac{F(t_n,t)}{1+\alpha^2}\right]\mathbf{H}\times\mathbf{M}_n-\right.$$

$$\left.-\cos\left[\frac{F(t_n,t)}{1+\alpha^2}\right]\mathbf{H}\times(\mathbf{H}\times\mathbf{M}_n)\right\},$$

$$C = \left\{|\mathbf{H}| + \mathbf{H}\mathbf{M}_n - (\mathbf{H}\mathbf{M}_n - |\mathbf{H}|)\times\right.$$

$$\left.\times\exp\left[-\frac{2\alpha}{1+\alpha^2}F(t_n,t)\right]\right\}|\mathbf{H}|,$$

$$F(t_n,t) = \int\limits_{t_n}^t dt_1|\mathbf{H}(t_n,t_1)|,$$

where $\mathbf{M}_n = \mathbf{M}(t_n)$. Solution (10) is obtained by writing (1) in the cylindrical coordinates with z-axes directed on vector $\mathbf{H}$.

Magnetic vector field $\mathbf{H}(t_n,t)$ in (10) is an effective magnetic field from the previous step, i.e. $\mathbf{H}(t_n)$. Therefore, the additional time depending external magnetic field, $\mathbf{H}^{(ext)}(t)$, can be included as $\mathbf{H}(t_n,t) = \mathbf{H}(t_n) + \mathbf{H}^{(ext)}(t)$. Field $\mathbf{H}^{(ext)}(t)$ can be used for the simulation of the magnetic writing process, or for the simulation of the neighbor's magnetic elements influence within the array of patterned media.

We should emphasize that computer calculation of the sequence of one-fold integrals within formulas (7)–(9) is very fast. For small cylinder one need about 1 sec with computer of 1.2 GHz to calculate field in all grid points $\{r_i, \varphi_j, z_k\}$ for one iteration step. Naturally, computation time depends on the total grid number, big particles need a longer time. We used a combination of calculation with software written on FORTRAN and *"Mathematica"* languages.

The final magnetization (in zero field at $t \to \infty$) depends on the magnetization prehistory, i.e. on the initial distribution $\mathbf{M}_0$ and precise external magnetic pulse shape, $\mathbf{H}^{(ext)}(t)$. In this paper we do not discuss the dynamic processes, and set $\mathbf{H}^{(ext)}(t) = 0$. The following initial magnetizations are typically considered: 1) Random initial state is used for finding lowest minima of the Gibbs energy. It is also used for modeling of "erasing head" work, e.g. with fast laser heating of material above the Curie temperature [22]. 2) $\mathbf{M}_0 = \mathbf{M}_z = \{0,0,1\}$ and/or 3) $\mathbf{M}_0 = \mathbf{M}_r = \{1,0,0\}$ are used for modeling of transversal recording [23, 24]. 4) $\mathbf{M}_0 = \mathbf{M}_x = \{\cos\varphi, -\sin\varphi, 0\}$ is used for modeling of longitudinal recording [24].

The iterative method of LLG equation solution was firstly proposed for the cubic particle [25]. At this case complicated formulas (6)–(9) are replaced by more simple formulas for Fourier expansion in Cartesian coordinates. For small sizes cubic particles the remanent state has a flowerlike or vortex magnetization configuration, which is in a good agreement with many previous calculations and experimental results.

In contrast to cubic particles there are just a few results for the magnetic states in the small cylinder [1, 2, 26, 27]. Experimental results [12, 13] demonstrate that for cylindrical particles (with low anisotropy material) flowerlike configurations are not favorable. It can be understood along the line that magnetization tends to avoid magnetic charges except two topological "singularities" [1, 26, 27].

Typical lattice size in calculations was changed from to $20 \times 20 \times 20$ to $120 \times 120 \times 120$. Parameters of the

material varied within the region $Q \in [10^{-3}, 1]$, and the cylinder geometry varies among $\{a, h\} \in [\lambda, 30\lambda]$. The magnetic behavior of cylinder is related to size, aspect ratio a/h and the prehistory. Below we present the main results of calculations.

a) **Low anisotropy**, $Q \leq 10^{-2}$. With random initial conditions, (and/or with $\mathbf{M}_0 = \mathbf{M}_r$) the cylinder with $a, h \leq 30\lambda$ has stable configuration, i.e. vortex (Fig.1). Stability of the single magnetic vortex for small

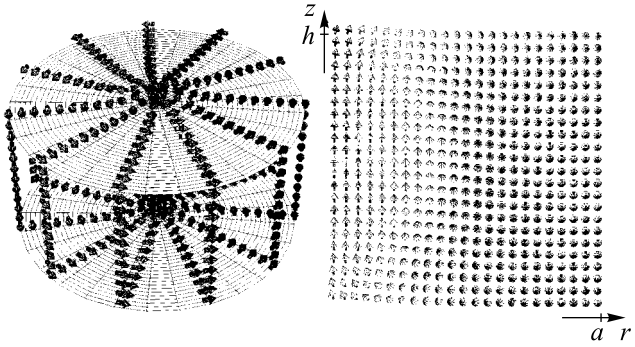

Fig.1. Side faces of the vortex configuration for a cylinder with $a = 5\lambda$, $h = 10\lambda$, $Q = 10^{-3}$. Cross section shows magnetization in $\{r, z\}$ plane. Random initial state

isotropic ferromagnetic cylinder was recently discussed in [28]. The vortex in Fig.1 has rather spiral structure, i.e. $M_r \neq 0$. Relative volume of homogeneous state with $M_z \approx 1$ increases with diminishing of the cylinder radius. As a result the flowerlike structure co-exists with the vortex solution for small cylinder at $a, h \leq 2\lambda$. With $\mathbf{M}_0 = \mathbf{M}_x$ for sufficiently big cylinders ($a > 10\lambda$) one can find the axially asymmetric solutions with spiral branches, similar to those which have been discussed in [29]. These solutions become more distinct with increasing of anisotropy.

b) **Intermediate anisotropy**, $10^{-2} < Q < 0.5$. With $a, h > 2\lambda$ magnetization tends to create magnetic bubble, with Bloch type domain wall, see in Fig.2. This magnetic bubble develops monotonically from the vortex state. With increasing radius, $a \geq 8\lambda$, two concentric domain walls appear, see in Fig.3. For tall cylinder with $a/h \ll 1$ and $a \geq 10\lambda$ the internal magnetic domains are forming around points of "singularity" ($r = 0$, $z = 0, h$) and do not grow inside the center of the cylinder. With longitudinal initial magnetization, $\mathbf{M_0} = \mathbf{M}_x$, and sufficiently large particles, $a \geq 30\lambda$, the complex magnetization configurations with broken axial symmetry may be developed. Another initial conditions, with non-zero radial component also yield complex multidomain structures for big particles. Domains can be formed in z directions. Vortex structure with different chirality on the

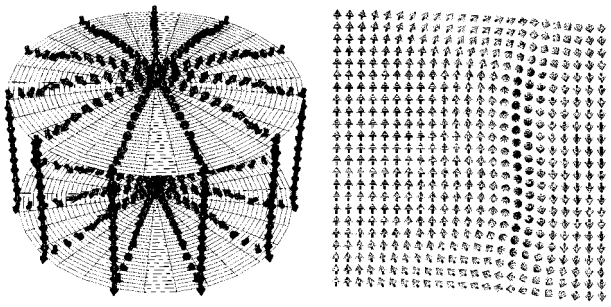

Fig.2. One-domain state with concentric Bloch wall along z direction. This wall is clearly seen in the $\{r, z\}$ cross-section. Input parameters are: $a = 5\lambda$, $h = 10\lambda$, $Q = 0.2$. Random initial state

top and the bottom can be obtained under initial state $\mathbf{M}_0 = \mathbf{M}_z$. Changing chirality occurs through nonsymmetrical Bloch domain wall, typical for weak anisotropy materials [1, 2]. This state seems to be metastable.

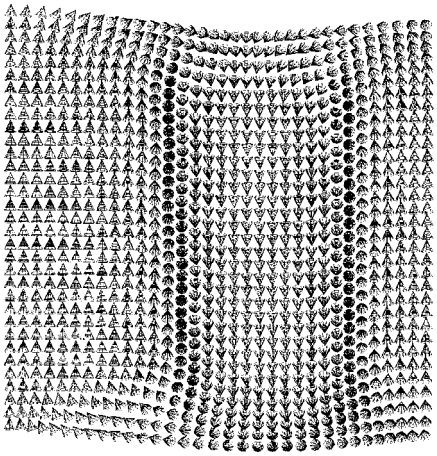

Fig.3. $\{r, z\}$ cross-section images two-domain structure with concentric Bloch domain walls. Parameters: $a = 10\lambda$, $h = 20\lambda$, $Q = 0.3$. Vortex initial state

c) **High anisotropy**, $Q \geq 0.5$. The "flower" state, Fig.4, is favourable for small cylinder under $\mathbf{M}_0 = \mathbf{M}_z$ initial condition. This configuration is stable with respect to small magnetic perturbations. One domain cylindrical particle has 'critical size', $a \approx 2\lambda$, when it stays 'uniformly' magnetized. It is near the limit of micromagnetic model validity. Thus, application of micromagnetic model for such sizes is questionable, it should be approved additionally by quantum mechanics calculations.

In conclusion, we have to say that the energetic consideration, which presents the "phase diagram" of different states in the particle [1, 2], sometimes insufficient for identification of states for magnetic recording problem. For example, authors [26] consider magnetic bubble im-

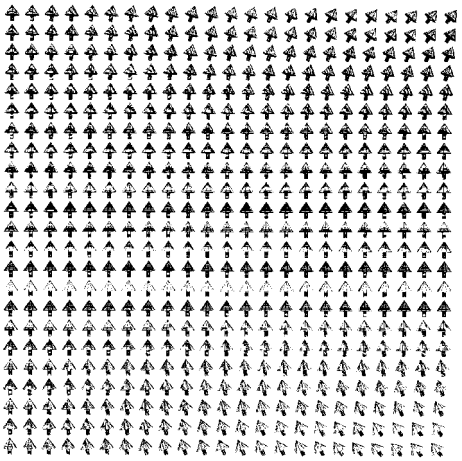

Fig.4. The 'flower' state. Parameters: $a = 5\lambda$, $h = 10\lambda$, $Q = 0.5$. Initial state $\mathbf{M}_0 = \mathbf{M}_z$

probable for the media with uniaxial anisotropy. Meanwhile integration of LLG equation demonstrates this state, Fig.2, on the contrary, is very probable for a wide class of initial conditions. Metastable states in magnetization can be separated sufficiently large energy barriers. These states present attractors with some "trapping region" with respect to the initial conditions. The dynamic theory, based on the solution of Landau-Lifshitz equation has no problem with identification of the corresponding states, while the pure energetic consideration that ignores the magnetization prehistory, may lead to some confusion.

The authors are very grateful to Profs. S. I. Anisimov and E. I. Katz for useful discussions.

1. A. Hubert and R. Shäfer, *Magnetic Domains. The Analysis of Magnetic Microstructures*, Springer Verlag, Berlin, Heidelberg, 1998.
2. A. Aharoni, *Introduction to the Theory of Ferromagnetism*, Oxford University Press, 2001.
3. J. F. Smyth, S. Schultz, D. R. Fredkin et al., J. Appl. Phys. **69**, 5262 (1991).
4. K. J. Kirk, J. N. Chapman, S. McVitie et al., J. Appl. Phys. **87**, 5105 (2000).
5. M. E. Schabes and H. M. Bertram, J. Appl. Phys. **64**, 1347 (1988).
6. W. Rave, K. Fabian, and A. Hubert, J. Magnetism & Magnetic Materials **190**, 332 (1998).
7. L. Folks and C. R. Woodward, J. Magnetism & Magnetic Materials **190**, 28 (1998).
8. E. Zueco, W. Rave, R. Shafer et al., J. Magnetism & Magnetic Materials **190**, 42 (1998).
9. W. Wulfhekel, H. F. Ding, W. Lutzke et al., Appl. Phys. **A72**, 463 (2001).
10. J. Lohau, A. Moser, C. D. Rettner et al., Appl. Phys. Lett. **78**, 990 (2001).
11. A. Fernandez, M. R. Gibbons, M. A. Wall, and C. J. Cerjan, J. Magnetism & Magnetic Materials **190**, 71 (1998).
12. C. A. Ross, M. Farhoud, M. Hwang et al., J. Appl. Phys. **89**, 1310 (2001).
13. A. Lebib, S. P. Li, M. Natali, and Y. Chen, J. Appl. Phys. **89**, 3892 (2001).
14. V. P. Puntes, K. V. Krishnan, and P. Alivisatos, Appl. Phys. Lett. **78**, 2187 (2001).
15. R. J. Gambino and T. Suzuki (Eds.), *Magneto-optical Recording Materials*, IEEE Press, New York, 2000.
16. E. M. Lifshitz and L. P. Pitaevsky, *Statistical Physics*, part 2, Pergamon Press, Oxford 1980.
17. J. Fidler and T. Schrell, J. Phys. D: Appl. Phys. **33**, R 135 (2000).
18. V. G. Baryakhtar, B. A. Ivanov, A. L. Sukstanskii, and E. Y. Melikhov, Phys. Rev. **B56**, 619 (1997).
19. W. Rave and A. Hubert, IEEE Trans. Magn. **36**, 3886 (2000).
20. W. Rave, K. Ramstöck, and A. Hubert, J. Magnetism & Magnetic Materials **183**, 329 (1998).
21. A. Thiaville, D. Tomas, and J. Miltat, Phys. Stat. Sol. **(a)170**, 125 (1998).
22. J. Gudde, U. Konrad, V. Jahuke et al., Phys. Rev. **B59**, R6608 (1999).
23. K. Okuda, K. Sueoka, and K. G. Ashar, IEEE Trans. Magn. **24**, 2479 (1988).
24. H. N. Bertram, *Theory of Magnetic Recording*, Cambridge University Press, 1994.
25. V. Ternovsky, J. P. Wang, and T. C. Chong, *Three-Dimensional numerical simulations in submicron-scale periodic magnetic arrays*, The 8-th MMM-Intermag Conference, San Antonio, Texas, USA, 2001, p. 340.
26. A. S. Arrott and T. L. Templeton, Physica **B233**, 259 (1997).
27. A. Hubert and W. Rave, J. Magnetism & Magnetic Materials **184**, 67 (1998).
28. K. Yu. Guslenko, and K. L. Metlov, Phys. Rev. **B63**, 100403(R), (2001).
29. A. B. Borisov, JETP Lett. **72**, 279 (2001).